THE UNUSUAL DISTRIBUTIONS OF IONIZED MATERIAL AND MOLECULAR HYDROGEN IN NGC 6881: SIGNPOSTS OF MULTIPLE EVENTS OF BIPOLAR EJECTION IN A PLANETARY NEBULA

G. RAMOS-LARIOS[1,3], M. A. GUERRERO[2], AND L. F. MIRANDA[2]

[1] Instituto de Astronomía y Meteorología, Av. Vallarta No. 2602, Col. Arcos Vallarta, C.P. 44130 Guadalajara, Jalisco, Mexico; gerardo@astro.iam.udg.mx
[2] Instituto de Astrofísica de Andalucía, IAA-CSIC, C/Camino Bajo de Huétor 50, 18008 Granada, Spain; mar@iaa.es, lfm@iaa.es

ABSTRACT

The planetary nebula NGC 6881 displays in the optical a quadrupolar morphology consisting of two pairs of highly collimated bipolar lobes aligned along different directions. An additional bipolar ejection is revealed by the hydrogen molecular emission, but its wide hourglass morphology is very different from that of the ionized material. To investigate in detail the spatial distribution of molecular hydrogen and ionized material within NGC 6881, and to determine the prevalent excitation mechanism of the H_2 emission, we have obtained new near-IR Brγ and H_2 and optical Hα and [N II] images, as well as intermediate resolution *JHK* spectra. These observations confirm the association of the H_2 bipolar lobes to NGC 6881 and find that the prevalent excitation mechanism is collisional. The detailed morphology and very different collimation degree of the H_2 and ionized bipolar lobes of NGC 6881 not only imply that multiple bipolar ejections have occurred in this nebula, but also that the dominant shaping agent is different for each bipolar ejection: a bipolar stellar wind most likely produced the H_2 lobes, while highly collimated outflows are carving out the ionized lobes into the thick circumstellar envelope. The asymmetry between the southeast and northwest H_2 bipolar lobes suggests the interaction of the nebula with an inhomogeneous interstellar medium. We find evidence that places NGC 6881 in the H II region Sh 2-109 along the Orion local spiral arm.

Key words: infrared: ISM – ISM: molecules – planetary nebula: individual (NGC 6881)

1. INTRODUCTION

Asymmetry is common among planetary nebulae (PNe) and it comes in a large variety of shapes and morphological features. On a large scale, the departure from symmetry goes from the mild asymmetry of elliptical PNe to the strong asymmetry displayed by bipolar PNe. Asymmetry in PNe is also revealed by an assortment of small-scale morphological features including the symmetric fast low-ionization emission regions (FLIERs) of elliptical PNe, as well as point-symmetric collimated outflows and their associated blowouts and bow-shock structures. The asymmetry in PNe has been linked on many occasions to binarity (e.g., Soker 2006), but there is no conclusive evidence supporting such a connection (Sörensen & Pollacco 2004; Bond 2000; Soker 1997, and references therein). On the contrary, the onset of bipolarity in PNe seems to require the evolution of a massive progenitor (e.g., Corradi & Schwarz 1995).

PNe that show asymmetric structures along different directions are of great importance, as the change in the direction of the ejection can be associated with the precession of the progenitor star in a binary system. This class of PNe is not homogeneous at all, and includes PNe with multiple collimated outflows along different directions (Corradi et al. 1997) or with precessing jet-like features (Miranda et al. 1999), starfish-shaped and multipolar PNe that show point-symmetric bow-shock features (Sahai & Trauger 1998; Sahai 2000), and quadrupolar and polypolar PNe with different sets of bipolar lobes aligned along different symmetry axes (Manchado et al. 1996; López et al. 1998). Polypolar and quadrupolar PNe are especially interesting as multiple hourglass structures imply recurrent bipolar ejections which are particularly difficult to interpret in the framework of

the interacting stellar wind model (Kwok et al. 1978; Balick 1987).

One of the most intriguing PNe with multiple bipolar lobes is NGC 6881. Originally classified as a quadrupolar PN, based on optical narrowband images and long-slit echelle spectra (Guerrero & Manchado 1998), NGC 6881 presents two pairs of highly collimated bipolar lobes with very similar, although not coincident, symmetry axes. The southwest lobe displays a loop-like feature that is highly reminiscent of a precessing collimated outflow, but its measured expansion velocity is low. Kwok & Su (2005) showed that the dense equatorial ring has recently changed its orientation, being aligned with the youngest pair of bipolar lobes.

Therefore, there are many signs suggesting that precession and sequential events of bipolar ejections have occurred in NGC 6881. The spatial distribution of the molecular hydrogen in this nebula, as revealed by near-IR narrowband H_2 (1–0) S(1) images (Guerrero et al. 2000), adds a new twist. Molecular hydrogen emission is detected in wide hourglass bipolar lobes that extend much farther than the ionized bipolar lobes. The H_2 bipolar lobes may represent a bipolar ejection unrelated to the formation of the two pairs of ionized bipolar lobes.

To study carefully the spatial distributions of ionized material and molecular hydrogen in NGC 6881 and to investigate the excitation mechanism of the H_2 molecule throughout the nebula, we have obtained new H_2, Brγ, [N II], and Hα images, and *JHK* intermediate-resolution long-slit spectroscopic observations. A description of the observations is presented in Section 2 and the results are given in Section 3. The results are discussed in Section 4, and the conclusions and a short summary are presented in Section 5.

---

[3] Visiting Astronomer, Instituto de Astrofísica de Andalucía.

Table 1
Narrow-Band Imaging of NGC 6881

Telescope	Filter	λ_c (Å)	$\Delta\lambda$ (Å)	Exp. time (s)
WHT	H$_2$(1−0)	21218	320	900
WHT	Brγ	21658	320	1000
WHT	Kc	22700	340	1000
NOT	[N II]	6589	9	1800
NOT	Hα	6568	8	900

Table 2
NIR Spectroscopic Observations of NGC 6881

Grism	λ (μm)	Dispersion (Å pix^{-1})	Slit width ('')	R	P.A. (°)	Exp. time (s)
JH	1.15−1.75	6.6	0.75	∼575	113	1800
K_B	1.92−2.34	4.3	0.75	∼1700	113	3000
K_B	1.92−2.34	4.3	0.75	∼1700	137	1200

2. OBSERVATIONS

2.1. Imaging

Narrowband near-IR images of NGC 6881 were obtained during 2006 September 9 using LIRIS (Long-Slit Intermediate Resolution Infrared Spectrograph) at the Cassegrain focus of the 4.2 m William Herschel Telescope (WHT) on Roque de Los Muchachos Observatory (ORM, La Palma, Spain). The detector was a 1k × 1k HAWAII array sensitive in the spectral range from 0.8 to 2.5 μm. The plate scale is 0''.25 pixel^{-1} and the field of view (FOV) is 4'.27 × 4'.27. The narrowband filters isolated the H$_2$ (1−0) S(1) 2.1218 μm and Brγ 2.1658 μm emission lines. An additional narrowband filter (Kc) centered at 2.270 μm was used in order to subtract the continuum contribution from the line emission detected through the H$_2$ and Brγ filters. The central wavelength and bandwidth of these filters are listed in Table 1.

We obtained series of 100 s exposures on each filter for the total integration times given in Table 1. The telescope pointing was shifted by a few pixels between each exposure, rastering the nebula to different locations on the detector. Each series of observations on the object was followed by a similar series of observations on adjacent blank sky positions. Individual exposures were flat-fielded and dark-corrected, and the sky frames were combined to obtain a master sky image. The images on the nebula were subsequently sky-subtracted, shifted, and averaged. The continuum contribution to the H$_2$ and Brγ emission was removed using the continuum Kc image. Since the H$_2$, Brγ, and Kc filters have very similar bandwidth, we do not find it necessary to scale the images, although differences in the point-spread function (PSF) of stars in the field of view required us to degrade the PSF of the H$_2$ image to match these of the Brγ and Kc images. The continuum subtracted H$_2$ and Brγ images and the Kc image are presented in Figure 1. The spatial resolution, as determined from the FWHM of stars in the FOV, is ∼0''.8.

Narrowband images in the [N II] and Hα emission lines were obtained on 2006 June 30 using ALFOSC (Andalucia Faint Object Spectrograph and Camera) at the 2.56 m Nordic Optical Telescope (NOT) in the ORM. The camera is a 2048 × 2048 CCD with a plate scale of 0''.19 pixel^{-1} and a FOV of 6'.5×6'.5. The [N II] and Hα images of NGC 6881 are also presented in Figure 1. The spatial resolution, as determined from the FWHM of stars in the FOV, was 0''.9.

2.2. Spectroscopy

Intermediate-resolution *JHK* long-slit spectroscopic observations were performed on 2004 July 2–4 using the NICS (Near Infrared Camera Spectrometer) at the 3.5 m Telescopio Nazionale Galileo (TNG) at the ORM. The NICS is a multi-mode instrument for IR observations (0.9−2.5 μm) that uses a HAWAII 1024 × 1024 array as detector. We used the LF camera,

providing a plate scale of 0''.25 pixel^{-1}, and the 0.75 slit, with a width of 0''.75 and a length of 4'. Observations were obtained using the *JH* and K_B grisms and the long-slit was placed along the central star at P.A.s 113° and 137° (Table 2). In order to provide the means for subtracting the sky emission, the nebula was placed at different positions along the slit.

The spectra were reduced using IRAF[4] routines of the noao.twodspec and noao.onedspec packages. The data were flat-fielded using dome flats, and the sky contribution was removed using sky spectra obtained at the same time as the nebular spectra. We used telluric sky lines for the wavelength calibration. The standard IR stars of spectral type A−A0 SAO 15832, SAO 48300, and SAO 72320 (Hunt et al. 1998) were used for the flux calibration. We obtained the sensitivity function by comparing the spectra of these stars with a blackbody model of temperature 9480 K, similar to the effective temperature of A0 stars. Finally, the telluric absorptions in the one-dimensional spectra of NGC 6881 were removed using the IRAF task "telluric," applying it to stars with featureless spectra in the *JHK* range.

3. RESULTS

3.1. Morphology

The notable differences in the spatial distributions of ionized material and molecular hydrogen within NGC 6881 described by Guerrero et al. (2000) are specially highlighted in the H$_2$, Hα, and [N II] composite picture shown in Figure 2. In NGC 6881, we can distinguish the following components.

3.1.1. The Equatorial Torus at the Central Region

The central regions of NGC 6881 contain both molecular and ionized material. This region can be described as a clumpy torus-like structure (Kwok & Su 2005) that is expanding at a moderate velocity (Guerrero & Manchado 1998). The details of the molecular and ionized material distribution in the central regions of NGC 6881, however, could not be studied properly by Guerrero et al. (2000), because of the limited spatial resolution of their near-IR images and poor continuum subtraction at this region. Our new continuum-subtracted H$_2$ image reveals two bright knots of H$_2$ emission located at the central region of NGC 6881 along its minor axis, suggesting a ring of molecular material. The relative distribution of ionized and molecular material in the central region of NGC 6881, shown in Figure 3, reveals that the H$_2$ emission encompasses the [N II] emission.

Molecular hydrogen in this region survives in a thin layer surrounding the ionized torus-like structure, most likely shielded by dense material from the ionizing flux of the central star.

Figure 1. Images of NGC 6881 in the Brγ (top, left), Kc (middle, left), and [N II] (bottom, left) narrowband filters. The images in the H₂ (top, right), [N II] (middle, right) and Hα (bottom, right) filters show a larger field of view than the images in the left column. The artifacts noticeable around the field stars in the continuum subtracted Brγ and H₂ images are residuals of the subtraction caused by a slight mismatch of the PSF between the line and continuum images. The arrows towards the northwest of the nebula in the right panels mark diffuse emission in the H₂, [N II], and Hα images associated with the northwest H₂ lobe and its northwest extension. The arrow towards the south of the nebula in the H₂ image marks diffuse emission unrelated to NGC 6881, probably a background galaxy.
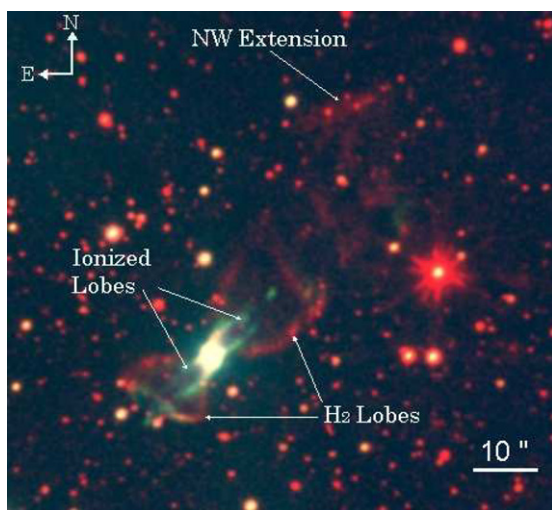
Figure 2. WHT LIRIS H_2 (red), and NOT ALFOSC $H\alpha$ (blue) and [N II] (green) composite picture of NGC 6881 overlaid with the different morphological features identified in the nebula.
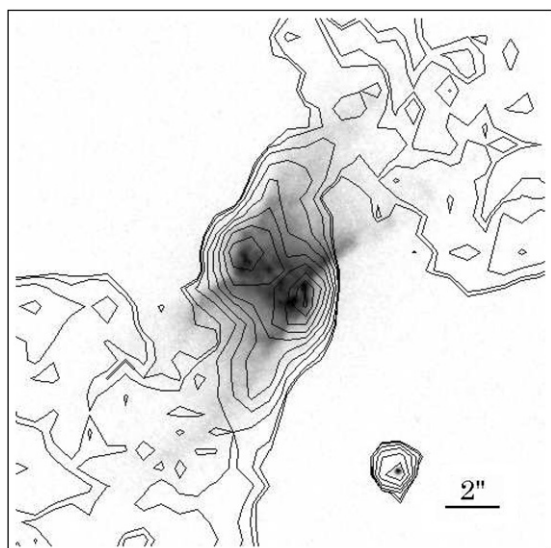

Figure 3. Expanded view of the central region of NGC 6881 in the *HST* WFPC2 [N II] image. The image is overlaid with H_2 contours extracted from the WHT LIRIS continuum-subtracted H_2 image.

3.1.2. The Highly Collimated Bipolar Lobes

The two pairs of highly collimated bipolar lobes are mainly detected in the $Br\gamma$, [N II], and $H\alpha$ images, while the H_2 emission from these lobes is weak. The northern wall of the northwest lobe is brighter than its southern wall, and the opposite applies to the southeast lobe, thus showing the point-symmetric brightness distribution typical of other bipolar PNe (e.g., K 4-55, Guerrero et al. 1996).

3.1.3. The Hourglass H_2 Bipolar Lobes

Contrary to the highly collimated bipolar lobes, the open hourglass bipolar lobes of NGC 6881 are dominated by H_2 emission.

They show a narrow waist coincident with NGC 6881 central regions and clear limb-brightening, indicating that they are formed by a thin layer of material.
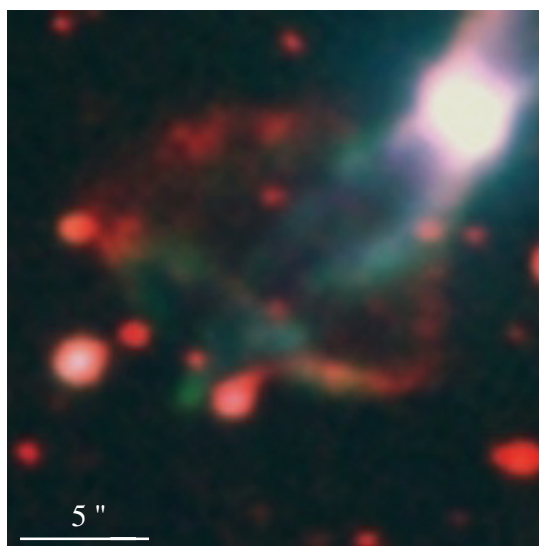

Figure 4. Expanded view of the southeast loop-like feature from the H_2, $H\alpha$, and [N II] composite picture of NGC 6881 (Figure 2).

The southeast lobe, extending $\sim 12''$, is smaller than the northwest lobe, with a size up to $\sim 20''$. There are notable differences between the tips of the southeast and northwest lobes. The tip of the southeast lobe is sharp and can be associated with the southeast loop-like structure detected in $H\alpha$ and very prominently in [N II] (Figure 4). The westernmost emission of the [N II] loop is coincident with the southwestern elbow of the H_2 lobe, and the [N II] loop structure traces closely the edge of the H_2 lobe. The northwest lobe does not have a sharp edge nor does it display a loop-like structure, but only a knot and a thin filament visible in the [N II] image located at its westernmost tip (Figures 1 and 2).

3.1.4. The Northwest Bipolar Lobe Extension

The H_2 emission of the northwest hourglass lobe displays an extension that casts its emission outwards up to $\sim 50''$ from the center of NGC 6881 along its symmetry axis. This emission is mainly detected in H_2, but there are also hints of [N II] and $H\alpha$ emission (Figure 2). The H_2 surface brightness of this feature is not homogeneous, but is distributed on a series of three bright bands interspersed between bands of diminished brightness. Interestingly, the bright bands can also be recognized in the $H\alpha$ image. The northwesternmost tip of these bands shows a remarkable wedge-shaped morphology.

3.1.5. Large-Scale Emission

The $H\alpha$ and [N II] images of NGC 6881 show large-scale diffuse emission, with the nebula laying on a broad arc of patchy emission that crosses the FOV from the northeast to the south (Figure 1). An examination of an $H\alpha$ image from the INT/WFC Photometric $H\alpha$ Survey (IPHAS) of the northern Galactic plane (Drew et al. 2005) of this region reveals a complex system of filaments. NGC 6881 ($l = 74°.5520$, $b = +02°.1137$) is projected along the local spiral arm onto the intricate network of $H\alpha$ filaments near the proximity of γ Cyg (e.g., Parker et al. 1979). In particular, NGC 6881 is projected towards the east of a large cavity of size $20' \times 12'$ oriented along the north–south direction that forms part of the H II region Sh 2-109 ($l = 79°.48$, $b = +00°.15$).
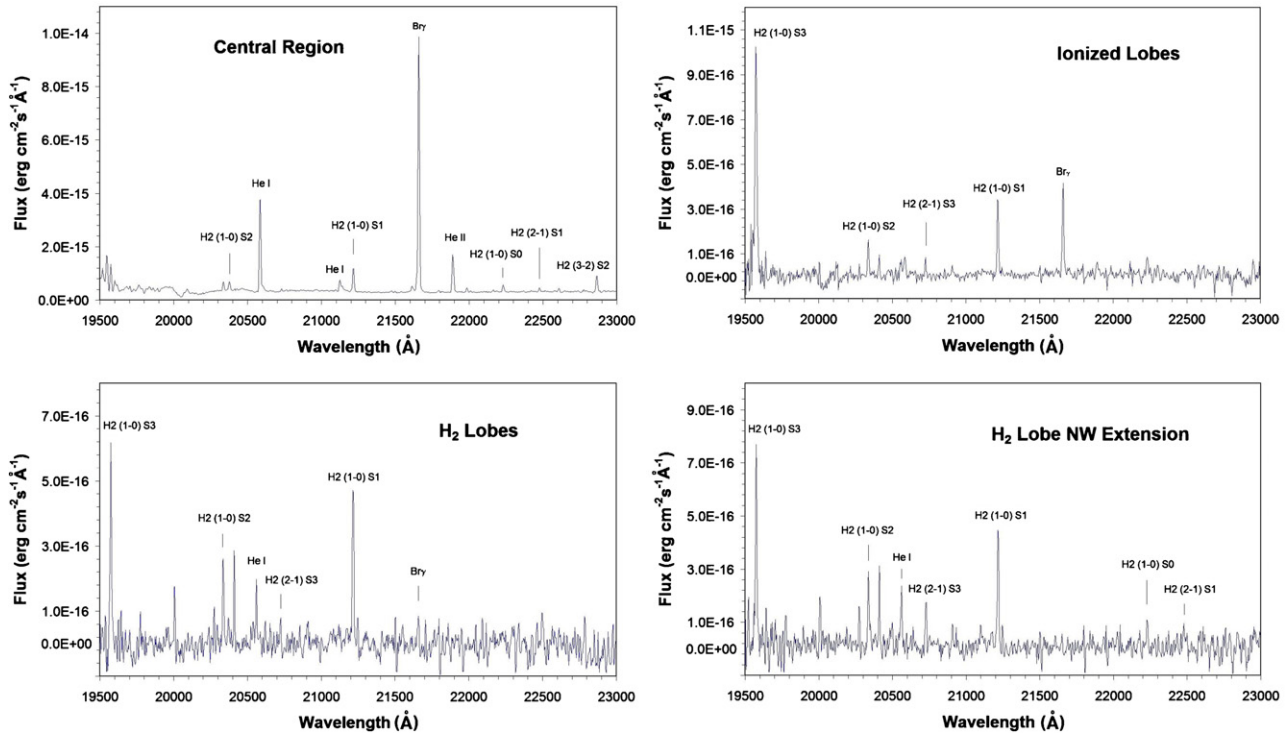
Figure 5. K_B spectra along P.A. = 137° of the central region, ionized lobes, H_2-dominated bipolar lobes, and northwest extension of the northwest H_2 bipolar lobe of NGC 6881. Line identifications are overlaid on the spectra.
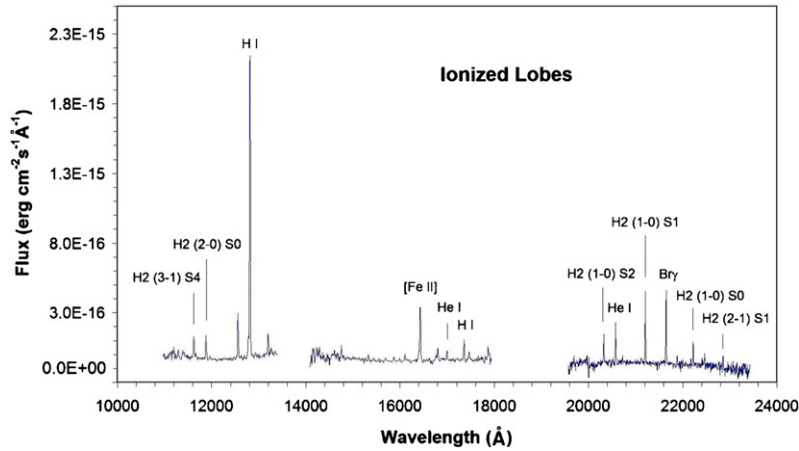

Figure 6. J, H, and K_B spectra along P.A. = 113° of the ionized lobes of NGC 6881. Line identifications are overlaid on the spectra.

3.2. Spectroscopic Analysis

The long-slit spectra of NGC 6881 detect continuum emission from the innermost regions and extended line emission all through the nebula. A preliminary inspection of the two-dimensional spectra reveals the variation at different locations of the nebula of important line ratios (e.g. H_2 1−0 S(1)/Brγ, He I/He II), in agreement with the different spatial distribution of emission shown by the Brγ and H_2 images. Guided by these images, we have extracted spectra from four individual regions: the central region, the ionized lobes, the H_2-dominated hourglass lobes, and the northwest H_2 lobe extension. The K spectra of these regions are shown in Figure 5, and the *JHK* spectra of the ionized lobes in Figure 6. Within our limited spectral resolution, the radial velocity derived for the different regions is similar.

The measured line intensities are listed in Tables 3 and 4. The spectra and line ratios confirm that the central region is Brγ-dominated, the ionized lobes show H_2/Br $\gamma \sim 1$, and the outermost regions are H_2-dominated. He II emission is confined to the central region, while the outermost regions show a wealth of H_2 lines. We note that the spectrum from the ionized lobes is most likely contaminated by emission from the H_2-dominated hourglass lobes.

3.3. H_2 Excitation

The molecule of H_2 can be excited by shocks or by UV fluorescence. The 1–0 S(1)/2–1 S(1) line ratio is traditionally used to diagnose the H_2 excitation mechanism, with a line ratio ~ 2 implying UV fluorescence (Black & van Dishoeck 1987),

Table 3
Line Fluxes at PA 137° with K_B Grism

λ (Å)	Line ID	Regions			
		Central regions	Ionized lobes	H₂ lobes	NW H₂ lobe extension
		($\times 10^{15}$ erg cm^{-2} s^{-1} Å^{-1})			
19446	Br8 H I	63	...	...	...
19549	He I	16	...	...	...
19574	H₂ (1,0) S(3)	12	17	11	9.2
19703	H₂ (8,6) O(2)	2.1	...	...	...
20338	H₂ (1,0) S(2)	4.2	2.1	3.8	4.6
20377	?	4.7	...	...	...
20587	He I	47	1.3	0.4	2.4
20732	H₂ (2,1) S(3)	1.2	0.8	1.3	2.8
20763	?	0.9	...	...	...
21126	He I	5.1	...	...	...
21138	He I	2.2	...	...	...
21218	H₂ (1,0) S(1)	12	4.7	5.6	6.2
21542	H₂ (2,1) S(2)	0.4	...	...	...
21614	He I ?	2.9	...	...	...
21658	Br7 H I (Brg)	110	5.5	1.3	...
21793	Br I	1.1	...	...	...
21887	He II	17	0.8	...	...
21985	?	2.1	...	...	...
22235	H₂ (1,0) S(0)	3.3	1.2	...	1.5
22477	H₂ (2,1) S(1)	1.6	...	...	1.0
22872	Br I ?	7.1	...	...	...

Table 4
Line Fluxes JH and K_B Grisms at PA 113°

λ (Å)	Line ID	Regions	
		Ionized lobes	H₂ lobes
		($\times 10^{15}$ erg cm^{-2} s^{-1} Å^{-1})	
10936	Pa 6 H I	160	...
11621	C I ?+ Fe I?	21	...
11666	H₂ (3,1) S(4), He I ?	4.5	...
11892	H₂ (2,0) S(0)	21	...
11970	He I	4.0	...
12566	[Fe II] ?, + Fe II ?	33	1.2
12784	He I	13	...
12817	Pa 5 (PaB) H I	190	11
13202	?	13	...
15335	Br 18 H I	2.3	...
15549	Br 16 H I	1.2	...
15693	Br 15 H I, H I 4-15	1.2	...
15875	Br 14 H I	1.1	...
15995	[Fe II]	1.0	...
16102	Br 13 H I, H I 4-13	2.5	...
16401	Br 12 H I, H I 4-12	2.6	...
16432	[Fe II]	15	...
16763	?	1.7	...
16801	Br 11 H I, H I 4-11, Fe I?	3.9	...
16997	He I	2.5	...
17356	Br 10 H I	5.5	...
17478	H₂ (1,0) S(7)	1.9	10
19570	H₂ (1,0) S (3) + [Fe II] ?	17	61
19703	H₂ (8,6) O (2)	1.1	...
20338	H₂ (1,0) S(2)	3.0	7.7
20580	He I	4.6	...
20656	H₂ (3,2) S(5)	0.5	...
20732	H₂ (2,1) S(3)	0.8	...
21133	He I	0.7	1.6
21218	H₂ (1,0) S (1)	6.8	11
21658	Br 7 (Brg) H I	7.4	0.9
21892	He II	0.9	...
21986	?	0.7	1.0
22014	H₂ (3,2) S(3)	1.0	...
22235	H₂ (1,0) S(0)	2.3	4.7
22477	H₂ (2,1) S(1)	1.2	1.7
22870	H₂ (3,2) S(2)	1.0	1.8

and a line ratio $\sim$10 implying shock excitation (Burton et al. 1989). The 1–0 S(1)/2–1 S(1) line ratio in the different regions of NGC 6881 ranges from 5.5 up to 7.5, thus indicating that shock excitation can be the most likely dominant excitation mechanism.

In a case of pure collisional excitation, the population of the energy levels of the H₂ molecule are described by a single-temperature Boltzmann distribution. To verify this statement, the excitation diagrams for several regions of NGC 6881 (Figure 7) have been calculated using a Boltzmann distribution of states where the column densities are related to the $\nu = 1$, $J = 3$ state by

$$\frac{g_3 N(\nu, J)}{g_J N(1, 3)} = \exp\left(-\frac{E(\nu, J) - E(1, 3)}{k T_{\text{ex}}}\right), \quad (1)$$

g_J and g_3 being the statistical weights. This equation can be rearranged in terms of the flux

$$\frac{F(\nu', J')\nu_{1,0S(1)} A_{1,0S(1)} g_3}{F(1,3)\nu_{\Delta\nu, \Delta J} A_{\nu', J' \to \nu'', J''} g_J} = \exp\left(-\frac{E(\nu, J) - E(1,3)}{k T_{\text{ex}}}\right), \quad (2)$$

where $A_{\nu', J' \to \nu'', J''}$ represent the transition probability, and $F(\nu', J')$ is the observed flux at frequency $\nu_{\Delta\nu, \Delta J}$.

The temperature can be inferred from the slope of the line fitted to the data points in Figure 7. In NGC 6881, the value of the vibrational excitation temperature, $T_{\text{ex}}(\nu)$, is similar to this of the rotational excitation temperature, $T_{\text{ex}}(J)$, and thus it can be concluded that shocks are the dominant excitation mechanism of H₂. The excitation temperature is 2100 K for the central region, 2200 ± 100 K for the ionized and H₂ lobes, and 2700 ± 100 K for the extension of the NW H₂ lobe. There is thus a trend for the temperature to increase as we move farther from the central regions of NGC 6881.

4. DISCUSSION

4.1. Ionized and Molecular Gas in NGC 6881

The H₂ emission of bipolar PNe is typically found in their equatorial rings and on the walls of their bipolar lobes, outlining closely the distribution of ionized material shown in Hα or [N II] images (Kastner et al. 1996; Guerrero et al. 2000). In NGC 6881, however, the different spatial distributions of ionized material and molecular hydrogen trace distinct nebular structures. A search in the literature shows that there are very few cases of bipolar PNe and proto-PNe in which the H₂ and Hα or [N II] morphologies are different: CRL 2688, M 2-9, NGC 2440, NGC 7027, J 900, and Hb 12. From this short list, NGC 2440 has to be discarded as recent *HST* images (Proposal ID. 11090) have shown that the H₂ arc seen by Latter et al. (1995) follows the outermost Hα emission. In CRL 2688 (the Egg Nebula), the H₂ emission is distributed along the equatorial plane and at the tips of the bipolar lobes seen in scattered light (Latter et al. 1993; Sahai et al. 1998). The H₂ bipolar lobes of M 2-9 envelop the bipolar lobes seen in emission lines of ionized species such as Fe II (Smith et al. 2005). The four-lobed shell of H₂ in NGC 7072 surrounds its elliptical ionized core, revealing the location of a
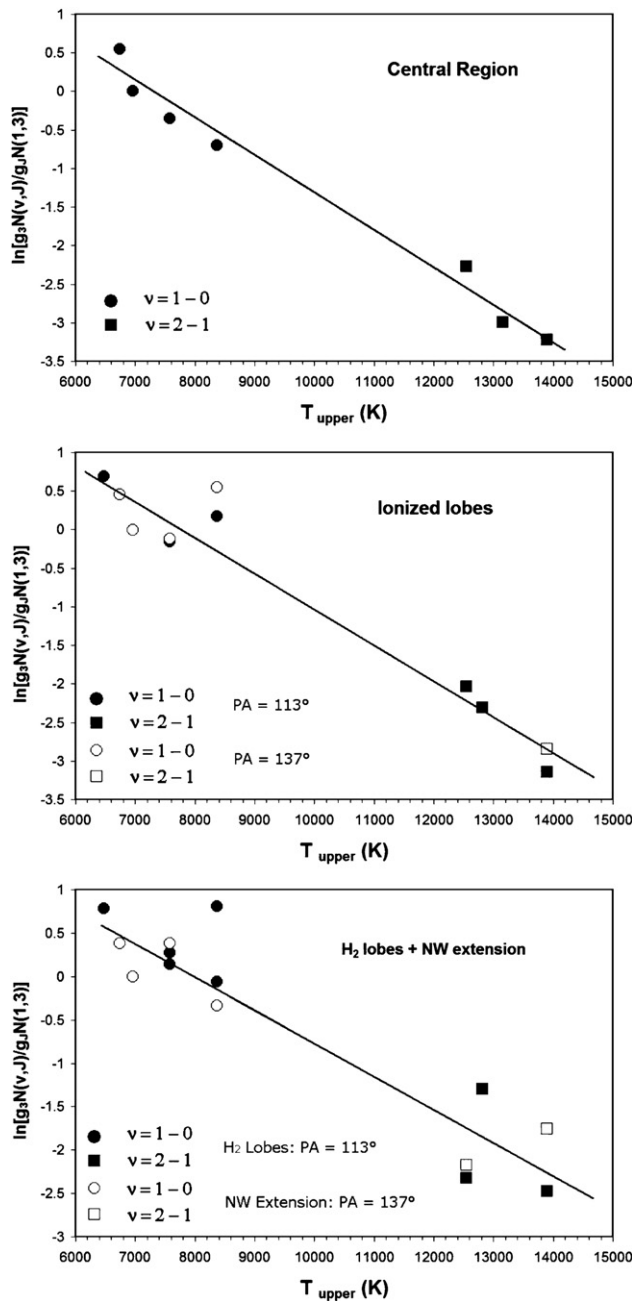
Figure 7. Excitation diagrams for the central region (top), ionized lobes (center), and H$_2$-dominated lobes and northwest extension (bottom) of NGC 6881. The diagrams show the upper state vibration-rotation populations relative to the $v = 1$, $J = 3$ level plotted against the upper state energy. The linear fits to the populations of different vibrational levels find rotational excitation temperatures of 2000 K, 2100 K, and 2700 K for the central region, ionized lobes, and H$_2$-dominated lobes and northwest extension, respectively.

photodissociation region (PDR) that is excited by the absorption of UV photons (Hora et al. 1999; Latter et al. 2000). In J 900, the H$_2$ emission shows a linear structure extending $\sim 40''$ that ends in an arc-like structure (Shupe et al. 1995; Latter et al. 1995). This feature has been suggested to be caused by UV excitation of stellar radiation that leaks out through holes in the nebular envelope (Shupe et al. 1995). Finally, the inner ionized bipolar lobes of Hb 12 are surrounded by an H$_2$ eye-shaped structure that is interpreted as a broad equatorial ring and a larger pair of

bipolar lobes (Hora & Latter 1996; Welch et al. 1999; Kwok & Hsia 2007).

Therefore, among the "exclusive" group of PNe with different distributions of H$_2$ and ionized gas, M 2-9, Hb 12, and NGC 6881 have ionized bipolar lobes that are enclosed within H$_2$ bipolar lobes. We note, however, that Hb 12 is a notable case of UV-excited fluorescent H$_2$ emission (Luhman & Rieke 1996; Hora & Latter 1996) and the same is suspected for M 2-9 (Smith et al. 2005), while NGC 6881 is representative of collisionally excited H$_2$ emission. The presence of multiple pairs of bipolar lobes in PNe is further discussed in the following section.

4.2. Multiple Bipolar Ejections in NGC 6881

The occurrence of multiple ejections of material is common among PNe, particularly among type I multiple-shell PNe that show faint, giant haloes (Chu et al. 1987). The haloes, interpreted as the relic of late thermal-pulse episodes (Stanghellini & Pasquali 1995; Hajian et al. 1997), are mainly associated with elliptical or round PNe, but are rare among bipolar PNe. Recurrent bipolar ejections resulting in multiple independent pairs of bipolar lobes have been reported for only a handful of PNe. The different pairs of bipolar lobes may have similar morphology and orientation, e.g., M 2-9 (Balick 1999; Schwarz et al. 1997), but in most cases they show notable differences, either affecting their morphology and degree of collimation, e.g., Mz 3 (Guerrero et al. 2004; Santander-García et al. 2004), the orientation of their symmetry axes, e.g., M 2-46 (Manchado et al. 1996), or its ionization degree, e.g., Hb 12 (Welch et al. 1999). In NGC 6881, we find two pairs of highly collimated ionized lobes oriented along slightly different directions and a pair of H$_2$ bipolar lobes with an open hourglass morphology.

The two pairs of ionized lobes of NGC 6881, first reported by Manchado et al. (1996), have been described in detail by Guerrero & Manchado (1998) and Kwok & Su (2005). Precession is evidenced by the different symmetry axes of each pair of ionized lobes and from the alignment between the equatorial ring and the youngest pair of bipolar lobes. The sharp morphology, similar kinematical age, and different orientation of the two pairs of bipolar lobes point to a sudden collimated ejection of material that has carved out bipolar cavities into the surrounding medium. The morphology of the ionized bipolar lobes of NGC 6881 is very reminiscent of the proto-PN CRL 618 in which high-velocity jets moving along different directions (Cox et al. 2003) have produced bipolar cavities in the nebular envelope (Trammell & Goodrich 2002). The similarities between the two bipolar nebulae extend to the coaxial rings of the bipolar cavities and to the bright, compact knots at their tips. The collimated outflows of CRL 618 might well evolved in the future into bipolar lobes similar to those of NGC 6881.

The limb-brightened morphology of the H$_2$ lobes indicates that the material is mainly confined in their walls, thus suggesting that the bipolar lobes carry enough momentum to sweep up and press the circumstellar medium into a thin sheet. Indeed, the prevalent shock excitation of H$_2$ requires a source of momentum. It is unlikely that a current fast ($\sim$1000 km s^{-1}) wind from the central star would provide this momentum, as such a stellar wind would be trapped by the inner ionized lobes. Our spectra do not provide information on the expansion velocity of the H$_2$ lobes, but an upper limit can be derived assuming that the [N II] emission from the loop-like structure at the edge of the southeast lobe is produced by a shock. For a planar shock to be able to produce significant [N II] λ6584 Å emission, but

low or minimal [O III] λ5007 Å emission (Guerrero & Manchado 1998), the shock velocity must not exceed $\sim$60 km s^{-1} (Hartigan et al. 1987). Such high speed makes unlikely the origin of the momentum in the thermal pressure of hot gas within the bipolar lobes. However, the momentum of the H$_2$ bipolar lobes must have been provided at the ejection time, either in a sudden bipolar ejection or through a stellar wind intrinsically bipolar or isotropic but collimated by an equatorial structure. The oblique shock of a bipolar lobe expanding at $\sim$60 km s^{-1} would be able to shock excite the H$_2$ molecules along its edge, while giving rise to [N II] and Hα emission at its tip. Such ballistic ejection may also explain the increasing H$_2$ temperature excitation with the distance to the nebula center.

The very different collimation degree of the ionized and H$_2$ lobes of NGC 6881 suggests that they formed during two different ejection events with substantial changes in the collimation conditions or even in the collimation mechanisms between the two episodes. The H$_2$ lobes formed very likely by the action of an episodic wind producing an hourglass-shaped ejection, while high velocity jets ejected along close directions produced the two pairs of ionized lobes. An additional period of isotropic heavy mass loss resulting in a dense envelope is revealed by concentric arcs detected around the innermost regions of NGC 6881 (Corradi et al. 2004).

4.3. NGC 6881 and the Surrounding Interstellar Medium

The morphology of the southeast and northwest H$_2$-dominated bipolar lobes are discrepant, with the former being smaller than the latter and showing a sharp edge at its southeast tip. This sharp edge is spatially coincident with a [N II] loop-like feature (Figure 4), a structure that has been interpreted as a low velocity precessing jet (Guerrero & Manchado 1998), but that, in view of the perfect spatial coincidence with the southeast tip of the H$_2$ lobe, seems more likely to mark its termination. The abrupt border of the southeast H$_2$ lobe and the [N II] loop-like structure may unveil the interaction of this bipolar lobe lobe with dense material.

As we noted in Section 3.1, NGC 6881 is embedded within diffuse emission that forms part of Sh 2-109, an inhomogeneous H II region located at a distance of 1.4 ± 0.4 kpc and with a diameter of 400 ± 100 pc (Fich & Blitz 1984). In view of the hint of interaction of the southeast H$_2$ lobe of NGC 6881 with dense material, resulting in the notably different morphologies of the southeast and northwest lobes, it is worthwhile to investigate the physical association of NGC 6881 with Sh 2-109. The distance to NGC 6881 has been estimated to be 2.5 kpc by Cahn et al. (1992) who used the Shklovsky method according to the Daub scheme. In their work, Cahn et al. used an angular radius of 2″.5 which seems inadequate as it only traces the bright, central regions of NGC 6881. This region has an angular radius $\sim$1″.2, but if we account for the ionized bipolar lobes, then an averaged angular radius of 6″.5 has to be used. If we adopt this radius, then the revised distance to NGC 6881 using the Cahn et al. method would be $\sim$1.5 kpc, supporting its physical association with the H II region Sh 2-109.

An inspection of IPHAS Hα images of this region reveals that the diffuse emission in which NGC 6881 is embedded constitutes the eastern wall of a large cavity-like structure. H I 21 cm line observations of the neutral gas distribution and kinematics of the region confirm that this structure is a cavity with an expansion velocity $\sim$10 km s^{-1} (Cappa et al. 1996). The radial velocity of this H I cavity, $v_{\rm LSR} \sim$ +16 km s^{-1}, is very similar to the radial velocity of NGC 6881, $v_{\rm LSR} \sim$ +2

km s^{-1} (Guerrero & Manchado 1998). The projection of the nebula onto the H I cavity and their similar radial velocities suggest that NGC 6881 may be located within this cavity, with its H$_2$-dominated southeast lobe hitting onto the dense material at the wall of the cavity, slowing it down and producing a sharp edge, while the northwest H$_2$ lobe expands into the H I cavity with little opposition.

5. CONCLUSIONS AND SUMMARY

New images and near-IR spectra of NGC 6881 confirm the different distribution of ionized material and molecular hydrogen within this PN. The H$_2$ images have resolved its central region which shows the spatial distribution expected for a ring of molecular material surrounding an innermost ionized ring. The H$_2$ bipolar lobes share the same orientation than the ionized lobes, but they are less collimated and display a distinct hourglass morphology. The H$_2$ emission is predominantly shock excited, both in the central ring and in the H$_2$ bipolar lobes.

We infer a complex history formation for NGC 6881, involving important changes in the collimation mechanism of the bipolar lobes in the latest evolutionary stages. The H$_2$ bipolar lobes are consistent with the action of a bipolar wind. The final evolution of the PN implied the ejection of episodic fast collimated outflows with changing directions that interacted with the dense circumstellar envelope ejected in a previous phase.

The southeast H$_2$ lobe of NGC 6881 is less extended than the northwest lobe and shows a sharp edge, implying the interaction of NGC 6881 with an inhomogeneous interstellar medium. We find very likely that NGC 6881 is within a cavity in the midst of the H II region Sh 2-109.

REFERENCES

Balick, B. 1987, AJ, 94, 617
Balick, B. 1999, in ASP Conf. Ser. 188, Optical and Infrared Spectroscopy of Circumstellar Matter, ed. E. Guenther, B. Stecklum, & S. Klose, (San Francisco, CA: ASP), 241
Black, J. H., & van Dishoeck, E. F. 1987, ApJ, 322, 412
Bond, H. E. 2000, in ASP Conf. Ser., 199, Asymmetrical Planetary Nebulae II: From Origins to Microstructures, ed. J. H. Kastner, N. Soker, & S. Rappaport, (San Francisco, CA: ASP), 115
Burton, M. G., Brand, P. W. J. L., Geballe, T. R., & Webster, A. S. 1989, MNRAS, 236, 409
Cahn, J. H., Kaler, J. B., & Stanghellini, L. 1992, A&AS, 94, 399
Cappa, C. E., Dubner, G. M., Rogers, C., & St-Louis, N. 1996, AJ, 112, 1104
Chu, Y.-H., Jacoby, G. H., & Arendt, R. 1987, ApJ, 64, 529
Corradi, R. L. M., Guerrero, M., Manchado, A., & Mampaso, A. 1997, in IAU Symp. 180, Planetary Nebulae, ed. H. J. Habing, & H. J. G. L. M. Lamers (Dordrecht: Kluwer Academic), 216
Corradi, R. L. M., Sanchez-Blázquez, P., Mellema, G., Gianmanco, C., & Schwarz, H. E. 2004, A&A, 417, 637
Corradi, R. L. M., & Schwarz, H. E. 2005, A&A, 293, 871
Cox, P., Huggins, P. J., Maillard, J.-P., Muthu, C., Bachiller, R., & Forveille, T. 2003, ApJ, 568, L87

Drew, J. E., et al. 2005, MNRAS, 362, 753
Fich, M., & Blitz, L. 1984, ApJ, 508, 262
Guerrero, M. A., Chu, Y.-H., & Miranda, L. F. 2004, AJ, 128, 1694
Guerrero, M. A., & Manchado, A. 1998, ApJ, 279, 125
Guerrero, M. A., Manchado, A., & Serra-Ricart, M. 1996, ApJ, 456, 651
Guerrero, M. A., Villaver, E., Manchado, A., García-Lario, P., & Prada, F. 2000, ApJS, 127, 125
Hajian, A. R., Frank, A., Balick, B., & Terzian, Y. 1996, ApJ, 477, 226
Hartigan, P., Raymond, J., & Hartmann, L. 1987, ApJ, 316, 323
Hora, J. L., & Latter, W. B. 1996, ApJ, 461, 288
Hora, J. L., Latter, W. B., & Deutsch, L. K. 1999, ApJS, 124, 195
Hunt, L. K., Mannucci, F., Testi, L., Migliorini, S., Stanga, R. M., Baffa, C., Lisi, F., & Vanzi, L. 1998, AJ, 115, 2594
Kastner, J. H., Weintraub, D. A., Gatley, I., Merrill, K. M., & Probst, R. G. 1996, ApJ, 462, 777
Kwok, S., & Hsia, C. H. 2007, ApJ, 660, 341
Kwok, S., Purton, C. R., & Fitzgerald, P. M. 1978, ApJ, 219, L125
Kwok, S., & Su, K. Y. L. 2005, ApJ, 635, L49
Latter, W. B., Dayal, A., Bieging, J. H., Meakin, C., Hora, J. L., Kelly, D. M., & Tielens, A. G. G. M. 2000, ApJ, 539, 783
Latter, W. B., Hora, J. L., Kelly, D. M., Deutsch, L. K., & Maloney, P. R. 1993, AJ, 106, 260
Latter, W. B., Kelly, D. M., Hora, J. L., & Deutsch, L. K. 1995, ApJS, 100, 159
López, J. A., Meaburn, J., Bryce, M., & Holloway, A. J. 1998, ApJ, 493, 803
Luhman, K. L., & Rieke, G. H. 1996, ApJ, 461, 298L

Manchado, A., Guerrero, M. A., Stanghellini, L., & Serra-Ricart, M. 1996, The IAC Morphological Catalog of Northern Galactic Planetary Nebulae (Tenerife: IAC)
Manchado, A., Stanghellini, L., & Guerrero, M. A. 1996, ApJ, 466, L95
Miranda, L. F., Guerrero, M. A., & Torrelles, J. M. 1999, ApJ, 117, 1421
Parker, R. A. R., Gull, T. R., & Kirshner, R. P. 1979, An Emission Line Survey of the Milky Way (NASA SP-434)
Sahai, R. 1998, ApJ, 537, L43
Sahai, R., Hines, D. C., Kastner, J. H., Weintraub, D. A., Trauger, J. T., Rieke, M. J., Thompson, R. I., & Schneider, G. 1998, ApJ, 492, L163
Sahai, R., & Trauger, J. T. 1998, AJ, 116, 1357
Santander-García, M., Corradi, R. L. M., Balick, B., & Mampaso, A. 2004, A&A, 426, 185
Schwarz, H. E., Aspin, C., Corradi, R. L. M., & Reipurth, B. 1997, A&A, 319, 267
Shupe, D. L., Armus, L., Mattews, K., & Soifer, B. T. 1995, AJ, 109, 1173
Smith, N., Balick, B., & Gehrz, R. D. 2005, AJ, 130, 853
Soker, N. 1997, ApJS, 112, 487
Soker, N. 2006, PASP, 118, 260
Sörensen, P., & Pollacco, D. 2004, in ASP Conf. Ser. 313, Asymmetrical Planetary Nebulae III: Winds, Structure and the Thunderbird, ed. M. Meixner, J. H. Kastner, B. Balick, & N. Soker, (San Francisco, CA: ASP), 515
Stanghellini, L., & Pasquali, A. 1995, ApJ, 452, 286
Trammell, S. R., & Goodrich, R. W. 2002, ApJ, 579, 688
Welch, C. A., Frank, A., Pipher, J. L., Forrest, W. J., & Woodward, C. E. 1999, AJ, 522, L69